An atomistic description of the nematic and smectic phases of 4-n-octyl-4′ cyanobiphenyl (8CB)

Mattia Felice Palermo, Antonio Pizzirusso, Luca Muccioli, and Claudio Zannoni

Citation: J. Chem. Phys. **138**, 204901 (2013); doi: 10.1063/1.4804270
View online: http://dx.doi.org/10.1063/1.4804270
View Table of Contents: http://jcp.aip.org/resource/1/JCPSA6/v138/i20
Published by the American Institute of Physics.

An atomistic description of the nematic and smectic phases of 4-n-octyl-4′ cyanobiphenyl (8CB)

Mattia Felice Palermo, Antonio Pizzirusso, Luca Muccioli, and Claudio Zannoni[a)]
Dipartimento di Chimica Industriale "Toso Montanari" and INSTM, Università di Bologna, Viale Risorgimento 4, IT-40136 Bologna, Italy

(Received 27 February 2013; accepted 21 April 2013; published online 22 May 2013)

We report the results of atomistic molecular dynamics simulations of 4-n-octyl-4′ cyanobiphenyl (8CB) on samples of 750 and 3000 molecules showing the spontaneous formation of the nematic phase and then of smectic layers by gradually cooling down from the isotropic phase. Orientational, positional, and mixed order parameters, layer spacing, translational diffusion tensor components and their temperature dependence are reported. A detailed comparison with available experimental data validates the model and force field employed and clarifies the molecular organization of this important liquid crystal often used as reference smectic material. © *2013 AIP Publishing LLC*. [http://dx.doi.org/10.1063/1.4804270]

I. INTRODUCTION

Atomistic simulations have recently started to offer a view with an unprecedent level of detail on the molecular organization and dynamics of condensed matter, and of liquid crystals (LC) in particular, allowing us to inspect for the first time the role of specific molecular features such as internal flexibility and charge distributions on the phase behavior.[1–6]

Compared with generic models, such as the Gay-Berne one,[7,8] where each mesogen molecule is replaced by a single rigid object, the atomistic level of description grants access to the chemical details needed to predict or at least interpret the results of X-ray diffraction, nuclear magnetic resonance (NMR), and other real experiments. For instance, several papers published in the last few years have proved that "*in silico*" nematics such as cinnamates[1] and cyanobiphenyls[5,9,10] can reproduce a large number of experimental results such as transition temperatures, density, order parameters, NMR dipolar couplings, and can help to interpret the origin of phenomena like the odd-even effect, i.e., the alternation in nematic-isotropic (NI) transition temperatures determined by the variation of the number of aliphatic carbon atoms in the homologue series of these LC compounds.

It is also worth pointing out that atomistic simulations have a significant predictive role: for example, simulated values of the fourth rank orientational order parameter $\langle P_4 \rangle$ obtained for 4-n-pentyl-4′-cyanobiphenyl were at variance with experimental ones available at the time of publication,[11] which were obtained from depolarized Raman scattering, but have more recently proved to be in good agreement with those obtained using an improved version of the same technique.[12] It should also be pointed out that it is quite common to find a relatively large scattering among measurements of structural and dynamic data published by different groups, even when the same characterization technique is nominally used, and that simulations can thus represent also a useful complement to experiment. In another context the advantages of combining experiments and predictive simulations have also been recently shown for NMR studies of solutes dissolved in nematics.[13,14]

While the quality of observable results obtained from molecular dynamics (MD) is approaching that of real experiments for nematics, much less is known on the possibility of reliably reproducing smectic molecular organizations and properties. From this point of view, 4-n-octyl-4′-cyanobiphenyl (8CB) is an ideal test bench system since it has been the subject of numerous experimental investigations and of one of the first atomistic studies a few years ago.[15] Even though such early simulations were started assuming molecules already placed in layers and their trajectories were followed for a time of a few nanoseconds, shorter than the expected rotational relaxation time for a molecule of the size of 8CB, more recently several groups have reported simulation results for the 8CB bulk phase.[16–19] McDonald and Hanna,[16] employing a united atom (UA) level of modeling, where CH, CH_2, and CH_3 groups are considered as suitably parameterized spherical interaction sites, successfully obtained a smectic phase from the isotropic even if, probably because of the choice of neglecting electrostatic interactions, they did not reproduce the transition temperatures (e.g., they obtained $T_{NI} > 400$ K) as well as the dimerization of 8CB molecules and thus the layer spacing observed through X-ray measurements.[20–22] De Gaetani and Prampolini,[17] employing a mixed UA – all atoms model, found the spontaneous onset of a partial bilayer smectic phase in a temperature range compatible with the experimental one, although the layer spacing was still rather far from the one obtained by X-ray measurements[20–22] and the limited number of simulations did not allow to precisely assess the transition temperatures. The simulation of cyanobiphenyls, particularly 5CB and 8CB has also been tackled by Zhang *et al.*,[18] with good estimated results for the transition temperatures, using a Force

a)Electronic mail: Claudio.Zannoni@unibo.it

Field (FF) obtained modifying the TraPPE-UA set[23] so as to reproduce the bulk density for 5CB within 2%.

Another recent work by Chami *et al.*[24] reported the simulation of Electron Paramagnetic Resonance (EPR) spectra of a cholestane nitroxide spin probe dissolved in 8CB starting from all atom MD simulations (thus explicitly including the hydrogens using AMBER parameters). While the simulated EPR spectra closely resemble the experimental ones, the transition temperatures ($T_{NI} \approx 375$ K, $T_{SN} \approx 340$–360 K) are still far from the experimental values ($T_{NI}^{exp} \approx 313.8$ K, $T_{SN}^{exp} \approx 306.5$ K).[25] Moreover, even though the onset of a partial bilayer smectic phase was observed both visually and from the calculation of the radial distribution function parallel to the director, $g_{||}(r)$, no estimation of the positional order parameter was reported.[24]

Here, we take advantage of the united atoms force field we have recently developed and validated for the nematic phase of cyanobiphenyls[10] to investigate in detail 8CB in its nematic and smectic phases. One of the significant issues we plan to examine is the type and extent of antiparallel arrangement for these molecules with a strong terminal dipole,[26] comparing with X-ray data. Another is the determination of positional and, for the first time, of the mixed positional-orientational order parameters, testing to what extent the two types of ordering can be considered independent as sometimes assumed in theoretical mean field models.[27] The third is to look at translational dynamics, and in particular to the diffusion coefficients for movements inside the layers and across, examining to what extent the UA approximation can affect a successful comparison with experimental studies.

II. METHODS AND COMPUTATIONAL DETAILS

We have run two series of simulations, the first one on systems with a number of molecules $N = 750$ at several temperatures, and the second one on a much larger system with $N = 3000$ to obtain a more in depth assessment of the positional order of the smectic phase and to study its dependence on the system size.

The 8CB molecules were modelled at UA level of detail using a AMBER-OPLS force field,[28,29] which was previously tuned in house to reproduce the experimental nematic-isotropic transition temperature of n-alkyl cyanobiphenyls with 5 to 8 carbon atoms in the linear alkyl chain[10] but that was not explicitly optimized for the smectic phase.

For the first series of simulations, we followed a previously established procedure:[6,10,30] we started from a temperature at which the sample is isotropic and then we progressively cooled it at lower temperatures, allowing to observe, if present, its spontaneous organization. Simulations were run in NPT conditions using NAMD[31] with multiple step integration: bonded, van der Waals, and electrostatic interactions were calculated every 2, 4, and 8 fs, respectively. The samples were kept at the constant pressure of 1 atm using a Berendsen barostat,[32] while the temperature, which ranged from 300 to 320 K, was kept constant through velocity rescaling.

To validate the computational assessment of the positional order, we have also run a second series of simulations and investigated three different N = 3000 molecules systems. One is a bulk sample at 300 K obtained by merging two previously equilibrated free standing 8CB thin films and removing the vacuum, obtaining a sample containing approximately 10 layers. This system was then brought to 310 K in order to investigate the gradual disappearance of the smectic order. We also studied a system obtained by merging 4 replicas of an isotropic system from the previous series of simulations and cooling it down to 300 K. The samples were kept at the constant pressure of 1 atm using a Langevin piston, allowing us to run simulations with the x and y axes of the cell kept at a constant ratio, thus maintaining a square section of the cell. Three-dimensional periodic boundary conditions were used in both two series of simulations and long range electrostatic interactions were computed through the Particle Mesh Ewald method.[33]

The average simulation runtime for each sample was about 150 ns long, a time much larger than the expected rotational and translational correlation decay times. It is worth noting that for N = 750 molecules samples at temperatures close to a phase transition, we prolonged the production time up to 400 ns, as far as we know, the longest ever used in MD liquid crystal studies.

III. RESULTS AND DISCUSSION

The liquid crystalline phase diagram of 8CB presents a nematic and a smectic mesophase in a very narrow temperature range (about 7 K), thus making its reproduction by means of MD simulations a challenging task. More specifically, the experimental smectic-nematic and nematic-isotropic transition temperatures (T_{SmN} and T_{NI}), which will be represented as vertical dashed lines in Figs. 1, 2, and 10, are located at 306.6 and 313.6 K respectively, thus a precision of about 1 K on the simulated results is required.

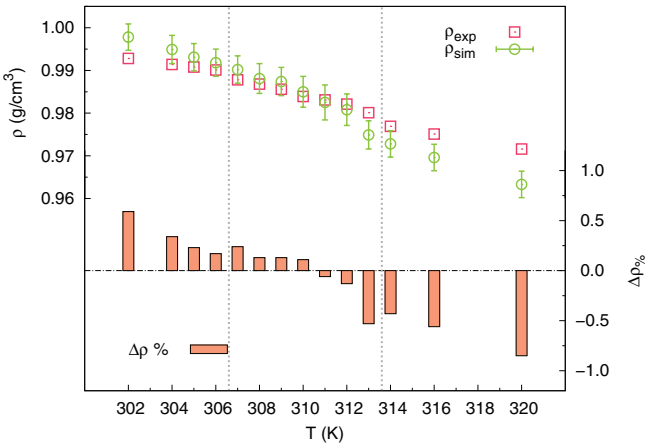

FIG. 1. Comparison between experimental[34] and simulated density as a function of temperature. $\Delta\rho_{\%}$ is the percent deviation of the simulated density from the experimental value. Vertical dashed lines represent the experimental transition temperatures T_{SmN} and T_{NI}.

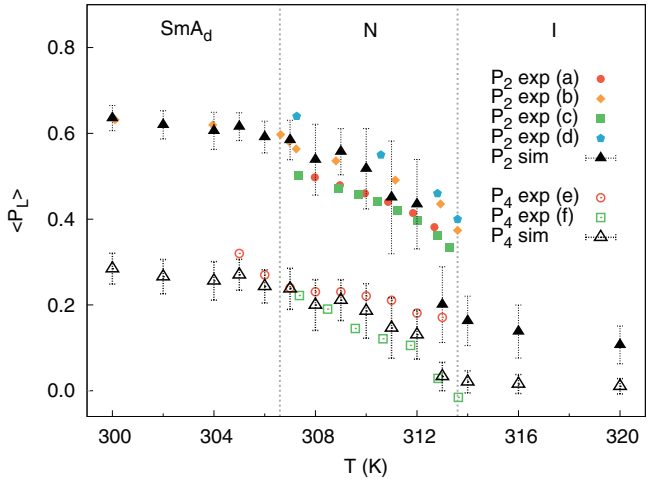

FIG. 2. Orientational order parameters $\langle P_2 \rangle$ and $\langle P_4 \rangle$ of the simulated sample compared to different sets of experimental data as a function of temperature. Data from refractive index measurements in Refs. 37–39 (a)–(c) and from polarized Raman spectroscopy measurements in Refs. 11 and 40 (d)–(f).

A. Density

A preliminary validation of our results for the N = 750 system can be found comparing density values obtained by our simulations with the experimental ones available in literature[34] (Fig. 1).

The simulated density decreases with increasing temperature, reproducing precisely the experimental trend, like already shown in Ref. 10 for smaller samples composed of 250 molecules. Still in Fig. 1, it can be noticed that the most accurate results are obtained in proximity of the experimental T_{NI}, with a deviation from the experiment not greater than 0.1%. Moving away from the transition region, this discrepancy increases to 1%, though these results still qualify as fairly accurate.

B. Characterization of molecular organizations

The system we wish to describe has nematic and smectic A phases and thus its molecules can possess both orientational and positional orders. If we approximate the molecules as uniaxial objects with orientation axis $\hat{u}$ (which is of course strictly not true, but reasonable in describing such complex mesogens with a minimal model) and we assume the liquid crystal to be cylindrically symmetric around a director z, then we can expand the probability distribution of finding a molecule at a certain position z and orientation β, $\cos\beta \equiv \hat{u} \cdot \hat{z}$, i.e., $P(z, \cos\beta)$ in an orthogonal basis of Legendre polynomials P_L and of Fourier harmonics $\cos q_n z$, $q_n \equiv 2\pi n/d$, with d a layer spacing, as[35,36]

$$P(z,\cos\beta) = \sum_{\substack{L=0 \\ n=0}}^{\infty} \frac{2L+1}{2d}(1+\delta_{L0}\delta_{n0})\, p_{L;n} P_L(\cos\beta)\cos(q_n z), \quad L \text{ even}, \tag{1}$$

with the normalization

$$\int_0^d \int_{-1}^{1} P(z,\cos\beta)\, dz\, d\cos\beta = 1. \tag{2}$$

The positional-orientational order parameters $p_{L;n}$ are defined from the expansion coefficients of $P(z, \cos\beta)$ as

$$p_{L;n} = \langle P_L(\cos\beta)\cos(q_n z)\rangle \tag{3}$$

and special cases are the orientational and positional order parameters: $\langle P_L(\cos\beta)\rangle$, $\langle \cos(q_n z)\rangle$. In particular, the isotropic-nematic thermotropic phase transition can be identified observing the variation with temperature of the averaged second Legendre polynomial $\langle P_2 \rangle$.

An additional way of characterizing the molecular organization of a fluid material is through pair distributions. The simplest is the radial distribution function $g_0(r)$:

$$g_0(r) = \frac{1}{4\pi r^2 \rho_N}\langle \delta(r - r_{ij})\rangle_{ij}, \tag{4}$$

where $\rho_N \equiv N/V$ is the number density of the sample, $\mathbf{r}_{ij}$ is the vector connecting the chosen reference centers of the i and j molecules.

For anisotropic systems it is also important to introduce the set of probability distributions of finding two molecules i, j at a certain distance and relative orientation from each other, $G_L(r)$, defined as

$$G_L^u(r) = \langle \delta(r - r_{ij}) P_L(\hat{u}_i \cdot \hat{u}_j)\rangle_{ij} / \langle \delta(r - r_{ij})\rangle_{ij}, \tag{5}$$

where $\hat{u}_i$, $\hat{u}_j$ are convenient unit vectors fixed on molecules i, j. In the uniaxial model $\hat{u}$ would just be the rod axis. In an atomistic simulation the choice of the reference centers and of the vector $\hat{u}$ is not univocal and actually in some cases it might be convenient to introduce more than one to give a more complete description. In Subsections III C–III I, we report our results for these one and two molecule properties.

C. Orientational order

For a uniaxial phase, the probability of finding a molecule at an angle β with respect to the phase director can be expanded in an orthogonal Legendre basis, a special case of Eq. (1), as

$$P(\cos\beta) = \sum_{L=0}^{\infty} \frac{2L+1}{2}\langle P_L\rangle P_L(\cos\beta), \quad L \text{ even}. \tag{6}$$

The second moment of the single molecule orientational distribution $\langle P_2 \rangle$, which is commonly used to characterize the average degree of alignment of a liquid crystal phase,[35] has been calculated in a rotationally invariant way through a standard procedure for liquid crystal simulation studies,[19] which requires to build and diagonalize an ordering matrix $\mathbf{Q}$, summing over all N molecules of the sample:

$$\mathbf{Q}(t) = \frac{1}{2N}\sum_{i=1}^{N}[3\hat{u}_i(t) \otimes \hat{u}_i(t) - \mathbf{I}], \tag{7}$$

where $\hat{u}_i$ is the chosen reference molecular axis and $\mathbf{I}$ is the identity matrix. The instantaneous scalar order parameter $P_2(t)$ can be obtained from the eigenvalues $\lambda_-(t)$, $\lambda_0(t)$, $\lambda_+(t)$, with $\lambda_-(t) < \lambda_0(t) < \lambda_+(t)$, of the $\mathbf{Q}$ matrix at time t. According to the most common convention, $P_2(t)$ corresponds to the largest eigenvalue, which is to say $P_2(t) = \lambda_+$, and once

a sufficiently long equilibrium trajectory is available, its overall average $\langle P_2 \rangle$ is calculated averaging over the production trajectory.

As can be seen in Fig. 2, at high temperatures the sample possesses a very low value of $\langle P_2 \rangle$, ranging from 0.1 to 0.2. Between 313 and 312 K we observe a steep rise of the order parameter, suggesting the spontaneous onset of a nematic phase. After the isotropic-nematic transition, $\langle P_2 \rangle$ increases from 0.4 to slightly less than 0.6 as we move toward the nematic-smectic transition.

Still in Fig. 2, the results obtained by our simulations can be compared with different sets of experimental data, in particular with birefringence and Raman depolarization spectroscopy measurements.[11,37–39] We notice that our simulated data are in good agreement with the average of the various, rather scattered experimental data sets.

The NI transition is characterized by considerable fluctuations of $\langle P_2 \rangle$, with a standard deviation comparable to the value of the order parameter itself (cf. the error bars in Fig. 2). This is due to the presence of order-disorder fluctuations during the time evolution of the sample and is consistent with the weak first order nature of the NI transition. We arbitrarily choose to consider a phase as definitely "ordered" when it shows a $\langle P_2 \rangle$ greater than 0.3, hence locating T_{NI} between 312 and 313 K. This assumption can be verified by plotting the histograms of $P_2(t)$ for all the configurations in each temperature run[19,41] (Fig. 3), allowing to easily spot the temperature at which the NI transition takes place. For temperatures above 313 K, it can be noticed how every sample possesses a broad distribution of $P_2(t)$, with a peak close to 0, highlighting how most of the configurations in those samples are isotropic. On the other hand, below 312 K the peaks are sharper and shifted toward high values of the order parameter, as a consequence of the onset of ordered liquid crystalline phases such as the nematic and smectic ones. The sudden inversion of the population of configurations possessing high or low $P_2(t)$ values taking place between 313 and 312 K confirms our estimate of the transition temperature, which is closer to the experimental value[42] of 313.6 K with respect to our previous simulation results of 317 K obtained on samples of 250 molecules.[10] This also indicates the importance of the sample size, which must be sufficiently large in order to accurately locate phase transitions. Below 308 K, the order parameter is almost constant with temperature and its fluctuations become much smaller, thus presenting sharper distributions.

The orientational order of the simulated samples was further investigated by studying the fourth rank order parameter $\langle P_4 \rangle$,[35] which is related to the fourth moment of the singlet orientational distribution and that can be calculated as follows:

$$\langle P_4 \rangle = \frac{1}{8N} \left\langle \sum_{i=1}^{N} (35 \cos^4 \beta_i - 30 \cos^2 \beta_i + 3) \right\rangle_t , \qquad (8)$$

where β_i is the angle between the reference axis of the ith molecule and the instantaneous phase director at time t. The value of $\langle P_4 \rangle$ at each temperature is compared in Fig. 2 with experimental data from Raman depolarization measurements:[40] it can be seen that the experimental trend is again well reproduced by simulations. Moreover, the profile of the fourth rank order parameter follows closely the one observed for $\langle P_2 \rangle$, dropping to zero above 312 K and thus confirming our previous estimate of the transition temperature.

D. Pair correlations

We start showing in Fig. 4 the radial distribution, $g_0(r)$, calculated here considering the center of charge of each molecule as the reference point (Fig. 5). Figure 4 shows the radial distributions of the smectic, nematic, and isotropic phases as a function of intermolecular separation r. It can be seen that each phase has a liquid-like distribution, characterized by the absence of peaks in the long range region and tending to its asymptotic value of 1 for r greater than 30 Å. In

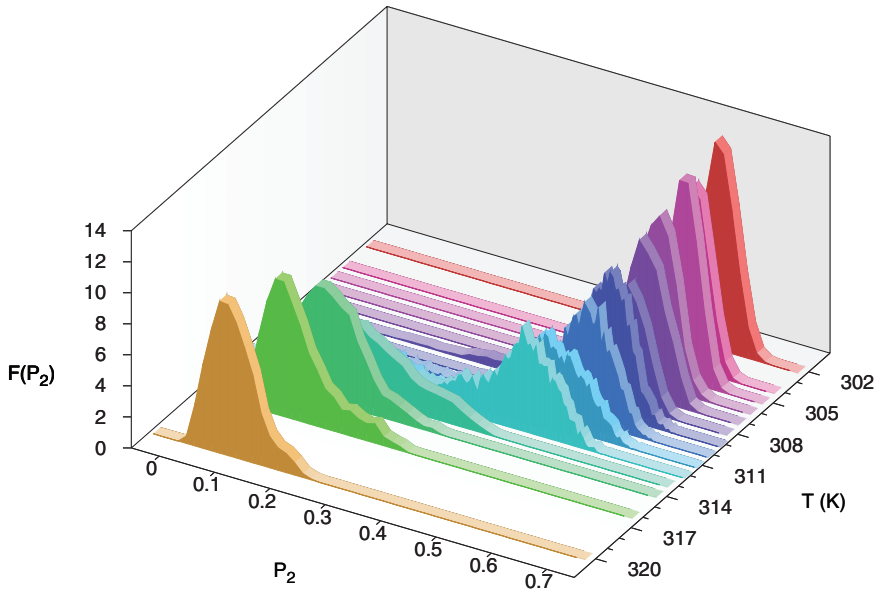

FIG. 3. Histograms of the instantaneous values of nematic order parameter $P_2(t)$ for all the configurations obtained in each temperature production run.

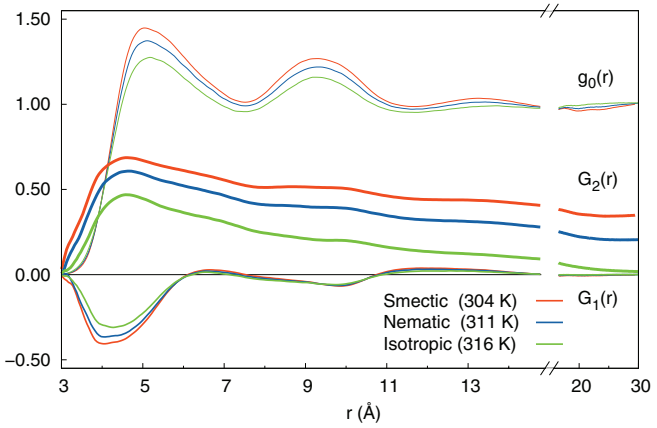

FIG. 4. Variation of the 8CB dipole orientational correlation functions $G_1(r)$, $G_2(r)$ and of the radial distribution of centers of charge, $g_0(r)$ for samples at 304, 311, and 316 K (representing the smectic, nematic, and isotropic phases, respectively).

the short range region though, each phase shows three distinct peaks, indicating the presence of local coordination shells. In particular, the first peak located at about 5 Å suggests the presence of quasi dimeric associations (as shown in Fig. 5) both in the isotropic and anisotropic phases, a common feature for systems composed of molecules bearing a strong terminal polar group. When the temperature is raised, the short range structure becomes less definite as shown by the radial distribution of the isotropic sample at 316 K.

Since we are particularly interested in the dipole organization, we have then evaluated the first and second rank positional-orientational distribution $G_L(r)$ choosing as reference vectors $\hat{u}_I$, $\hat{u}_J$, the electric dipole unit vectors $\hat{\mu}_I$, $\hat{\mu}_J$ in order to obtain the first and second rank distributions $G_1^{\mu}(r)$ and $G_2^{\mu}(r)$:

$$G_1^{\mu}(r) = \langle \delta(r - r_{ij})(\hat{\mu}_i \cdot \hat{\mu}_j)\rangle_{ij} / \langle \delta(r - r_{ij})\rangle_{ij}, \tag{9}$$

$$G_2^{\mu}(r) = \left\langle \delta(r - r_{ij}) \left[\frac{3}{2}(\hat{\mu}_i \cdot \hat{\mu}_j)^2 - \frac{1}{2}\right]\right\rangle_{ij} \Big/ \langle \delta(r - r_{ij})\rangle_{ij}, \tag{10}$$

where r_{ij} is now the distance between the charge centers of the i and j molecules.

In particular, the $G_1^{\mu}(r)$ function shown in Fig. 4 allows to clarify the local structure around each 8CB molecule. In the short separation region, a negative value for $G_1^{\mu}(r)$ is expected, since the first neighbouring molecules are oriented in an antiparallel fashion, thus yielding a negative average of $\hat{\mu}_i \cdot \hat{\mu}_j$. At a slightly greater distance, a change of sign of $G_1^{\mu}(r)$ is observed, as molecules belonging to the next coordination shell are in turn antiparallel to the ones in the first shell (thus parallel to the reference molecule). Between 8 and 14 Å, we observe the same trend as described for the first and second neighbours, but less pronounced since the influence of the reference molecule gets weaker as the distance increases. For long separations, the value of $G_L(r)$ tends to the limit of the square of the order parameter of rank L, $\langle P_L\rangle^2$ as shown in Refs. 35 and 41. Accordingly $G_1(r)$ tends asymptotically to 0 as the interaction with the reference molecular dipole becomes negligible, therefore, leading to a random head-tail orientation of most distant molecules.

The $G_2(r)$ function corresponds to evaluating the relative order parameter P_2 of a molecule with respect to the orientation of a reference molecule as a function of their intermolecular distance. Figure 4 shows the presence of a peak in the region $r \leq 5$ Å, corresponding to the short range orientational order arising from the packing interactions, in analogy with the behavior even found isotropic fluids.[9,26] At greater distances, in our case for $r > 30$ Å, $G_2(r)$ decreases and tends asymptotically to $\langle P_2\rangle^2$, the square of the order parameter of the phase.[41]

E. Smectic order parameter

It is well known that 8CB presents a smectic phase below 306.6 K.[42,43] To assess the validity of the force field developed in Ref. 10 also for these layered phases, we must determine whether the simulated sample is able to reproduce both the smectic-nematic transition temperature and properties such as the positional order parameter and layer spacing.

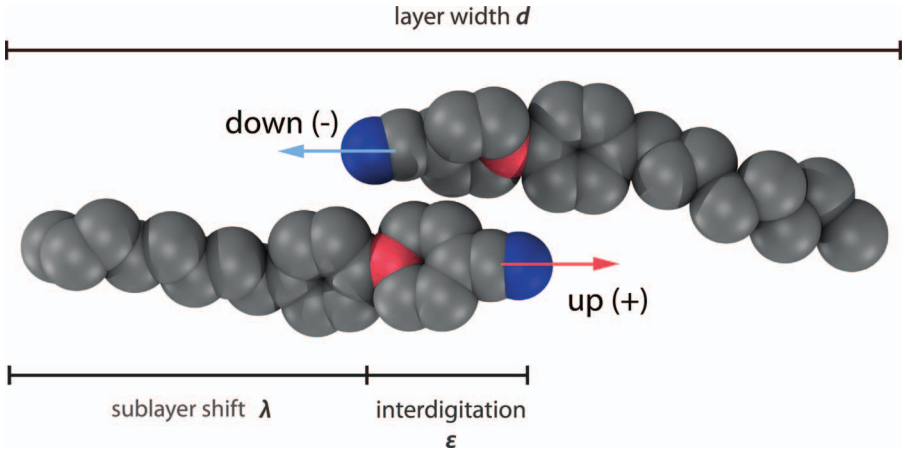

FIG. 5. The typical positional and orientational arrangement of neighbouring molecules belonging to two different sublayers in the SmA_d phase. d is the layer spacing and $\varepsilon = d - 2\lambda$ is the interdigitation. The center of charge, which turns out to be pretty conformation independent, is located on the red colored carbon atom.

To characterize the smectic phase of the simulated systems, it is important to correctly evaluate the positional organization to compare it with available experimental data. As of now, there is no standard method in literature to assess the positional order of smectic phases, thus we exploited 8CB simulated samples as a test bench to define a reliable protocol. Since we wish to assess the robustness of our results we have also studied, in addition to the $N = 750$ molecules sample at 300 K (which we will call system **a** from now on), three other larger bulk systems: (**b**) $N = 3000$ at 300 K obtained starting from a free standing thin film, (**c**) $N = 3000$ at 300 K obtained from an isotropic bulk sample, and (**d**) $N = 3000$ at 310 K obtained by heating a replicated sample of **a**.

These additional systems allow us to investigate the effect of the sample size and preparation on the positional order and, in particular, to consider the thermal history of the sample, i.e., how it was equilibrated before the onset of the smectic phase. This could be important also when trying to compare simulated properties to observed ones, since samples of smectics that present a nematic are usually experimentally prepared by cooling down a nematic sample which was previously aligned with an external field.

Going back to the description of positional order, we recall that for a uniaxial phase the probability of finding a molecule at a position z along the layer normal can be expanded in an orthogonal Fourier basis, again a special case of Eq. (1), as

$$P(z) = \frac{1}{d} + \frac{2}{d}\sum_{n=1}^{\infty} \tau_n \cos(q_n z), \tag{11}$$

where d is the layer spacing, $q_n \equiv 2\pi n/d$ and we have assumed the origin of the laboratory frame to be such that $P(z) = P(-z)$. τ_n is the nth positional order parameter, defined as

$$\tau_n = \int_0^d P(z)\cos(q_n z)\,\mathrm{d}z = \langle \cos(q_n z)\rangle, \quad n \geq 1, \tag{12}$$

where $\int_0^d P(z)\,\mathrm{d}z = 1$ and z gives the position of the center of mass of each molecule along the layer normal direction z, which is here assumed to be coincident with the phase director. This is appropriate for a smectic A and for our case as the smectic phase of 8CB is not found to be tilted either experimentally or in our simulations.

Notice that here we have considered that the coordinate system origin can be chosen at will, which is fine for theoretical treatments.[27,44,45] However, in a computer simulation the layers and thus the origin can fluctuate over time and we shall see in Appendix A that an appropriate treatment that gives τ_n in a translationally invariant way is essential to properly analyze simulated data. This is very much similar to obtaining an orientational order parameter in a rotationally invariant (scalar) form, as we have done before using the eigenvalues of the **Q** matrix. More specifically we have calculated $\tau_n$with two different methods, I and II, described in detail in Appendix A. The first method is a refinement of that used by De Gaetani and Prampolini[17] and Zhang *et al.*[18] who write the positional order parameters as

$$\tau_n = \sqrt{\langle \cos(q_n z)\rangle^2 + \langle \sin(q_n z)\rangle^2}, \tag{13}$$

while the second is based on the analysis of the translationally invariant two particle density autocorrelation (see Appendix A) $g(z_{12})$:

$$g(z_{12}) = 1 + 2\sum_{n=1}^{\infty} (\tau_n)^2 \cos(q_n z_{12}). \tag{14}$$

In Table I, we report the values of the main translational order parameter τ_1 for systems **a**, **b**, **c**, and **d** obtained with the two methods. It can be seen that the $N = 750$ molecules system **a** presents a lower τ_1 compared to the larger ones, while the smectic order in systems **b** and **c** is almost the same. The influence of the history and size of the sample on the layer spacing can be seen in Table I, where we also report the time average of d for each system. System **b** features the value of d closest to the experimental ones of $d = 31.4$[22]-31.7[46] Å, while in system **c** the layer spacing is lower. In system **a** we find a slightly higher value of d together with an order of magnitude higher uncertainty, probably due to the low number of layers.

TABLE I. Simulated values with respect to the temperature of: positional order parameter and layer spacing from method I: $(\tau_1)_I$, d; positional order parameters and layer spacing from method II: $(\tau_1)_{II}$, $(\tau_1^{\pm})_{II}$ and d_{gz}; shift between *up* and *down* sublayers λ; sublayer interdigitation ε; experimental layer spacing d_{exp}.

Sample	T (K)	N	$(\tau_1)_I$	d (Å)	$(\tau_1)_{II}$	$(\tau_1^{\pm})_{II}$	d_{gz} (Å)	λ (Å)	ε (Å)	d_{exp}[21]
a	300	750	0.13 ± 0.03	32 ± 1	0.12	0.28	32.3	14.4	3.6	31.2
b	300	3000	0.15 ± 0.01	31.3 ± 0.1	0.15	0.35	31.2	13.8	3.6	31.2
c	300	3000	0.15 ± 0.02	30.4 ± 0.2	0.14	0.33	30.4	13.5	3.4	31.2
d	310	3000	0.04 ± 0.01	26 ± 9	…	…	…	…	…	
	302	750	0.13 ± 0.02	32 ± 2	0.10	0.24	31.8	14.0	3.8	31.2
	304	750	0.12 ± 0.04	32 ± 2	0.10	0.23	32.3	14.2	4.0	31.2
	305	750	0.15 ± 0.03	32.5 ± 0.4	0.13	0.29	32.5	14.3	4.0	31.2
	306	750	0.13 ± 0.03	32.5 ± 0.9	0.11	0.25	32.6	14.3	3.9	
	307	750	0.12 ± 0.04	32 ± 1	0.11	0.24	32.6	14.3	4.0	
	308	750	0.10 ± 0.04	32 ± 2	0.07	0.16	31.9	14.1	3.7	
	309	750	0.10 ± 0.02	32 ± 2	0.07	0.17	31.8	14.0	3.7	
	310	750	0.08 ± 0.03	31 ± 3	0.07	0.16	31.9	14.1	3.7	
	311	750	0.04 ± 0.01	28 ± 5	0.05	0.11	31.6	14.0	3.5	

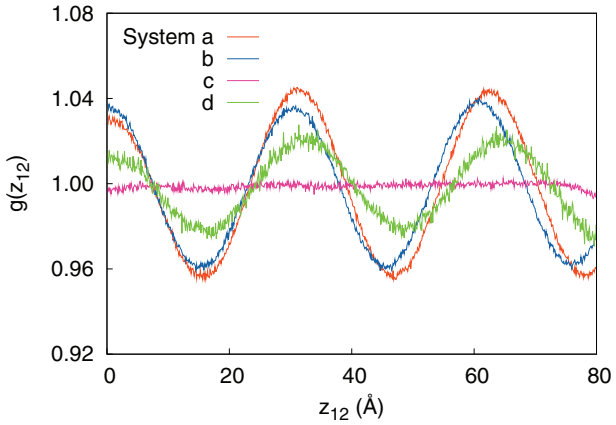

FIG. 6. The density autocorrelation $g(z_{12})$ for systems **a**, **b**, **c**, and **d**.

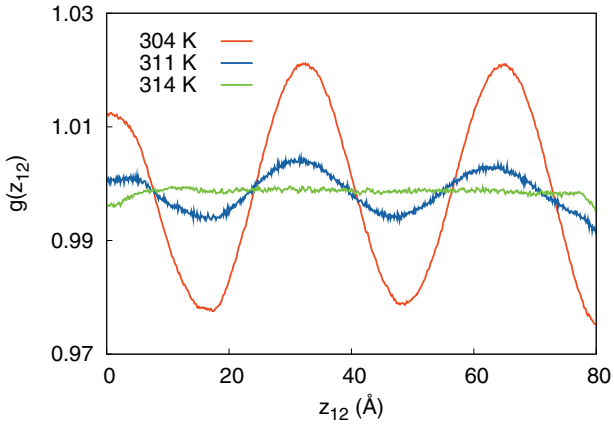

FIG. 7. Density correlation $g(z_{12})$ along the z axis for samples at 304, 311, and 316 K (representing the smectic, nematic, and isotropic phases, respectively).

In Fig. 6 it can be seen that, in agreement with the results obtained from method I, system **b** presents slightly higher layer spacing when compared to system **c**, once again highlighting the effect of the sample equilibration prior to the onset of the smectic phase. It can also be seen that system **a** features lower density oscillations and a higher value for the layer spacing. A flat $g(z_{12})$ trend can be observed for system **d**, suggesting the absence of positional order for the molecular centers of mass in the nematic sample at 310 K.

Comparing our results to those from other groups, we notice that the works from De Gaetani and Prampolini[17] and Zhang *et al.*[18] report a considerable discrepancy between the values of τ_1 calculated for small ($N < 1000$) and large ($N > 1000$) samples, while in our case the positional order parameter remains approximately the same regardless of the sample size (Table II). This highlights that the correction we propose in Appendix A, which takes into account the effect of the finite size of the system and the choice of the sampling region, is important for a correct evaluation of the positional order parameter.

For samples with $N > 1000$, we see that our results are in agreement with the ones from the two other groups. For these large systems, the corrections we proposed play indeed a small role since the size of the sample reduces the influence of the spurious term discussed in Appendix A and it can be assumed that the layer normals in Refs. 17 and 18 were close to one of the box axes. It must be noted that for both small and large systems, the value of the interlayer spacing d for our simulations is the closest to the experimental values,[22,46] while the value of τ_1 for all the large simulations is significantly lower than the experimental ones.[47,48]

We can now exploit the positional order parameter obtained to discuss the onset of the smectic phase, which experimentally occurs below 306.6 K[42] for 8CB. In Fig. 7, the $g(z_{12})$ functions for $N = 750$ samples at different temperatures are reported. At low temperatures the profile exhibits a clear sinusoidal trend, due to the presence of smectic layers. This behavior progressively disappears for samples at temperatures above 307 K. The trend is consistent with the one obtained for the values of τ_1 computed from methods I and II (Table I), which is gradually decreasing above 307 K and becomes negligible at 311 K. This result is in good agreement with the experimental smectic-nematic transition temperature of 306.6 K. It must be noted that in $N = 750$ sample, quite large smectic fluctuations are still present up to 311 K (Fig. 7 and Table I) while for the $N = 3000$ sample we find a truly nematic phase already at 310 K (Fig. 6 and Table I). This observation suggests that small size systems may favour positionally ordered phases above the smectic-nematic transition temperature. In any case, the presence of smectic fluctuations in the nematic temperature range is not surprising, as it has been already observed experimentally in several works.[46–50]

TABLE II. Comparison of the positional order parameter τ_1, the layer spacing d and second rank orientational order parameter $\langle P_2 \rangle$ from the most recent computational and experimental work available in literature. All atom, core, and N atoms refer to computations run on all atoms, on the phenyl core, and on the nitrogen atom only, respectively.

	N	T (K)	τ_1	d (Å)	$\langle P_2 \rangle$
This work (method I)	750	300	0.13 (all atom) 0.25 (core)	32	0.62
De Gaetani and Prampolini[17]	192	300	0.21 (all atom)	27	0.57
De Gaetani and Prampolini[17]	768	300	0.21 (all atom)	26	0.66
Zhang *et al.*[18]	256	300	0.21 (N atoms)	28	0.45
This work (method I)	3000	300	0.15 (all atom) 0.3 (core)	31.3	0.64
De Gaetani and Prampolini[17]	1536	300	0.14 (all atom)	27–28	0.68
Zhang *et al.*[18]	1024	300	0.32 (N atoms)	28.5	0.49
Alexander *et al.*[47] (neutron scattering)		293–305	0.46–0.57	31.5	
Kapernaum and Giesselmann[48] (X-rays)		292–309.5	0.64–0.74		

Since no evident discontinuity for τ_1 is present while heating the sample, a second order nature for the smectic-nematic transition can be assumed.

Regarding the interlayer distance, we can observe that below 307 K the simulated samples feature a d of about 32 Å (Table I), which is closer to the experimental value[46] of 31.7 Å with respect to previous simulation studies.[16–18] Besides, the interlayer distance obtained from simulations remains constant in the temperature range of the smectic phase, in agreement with the trend observed through X-rays measurements for 8CB by Urban and co-workers[21] and, recently for other smectics.[49]

F. Smectic A_d interdigitation

The smectic phase of 8CB, which belongs to the so-called SmA_d[51] category, is characterized by the presence of bilayers formed by two interdigitated sublayers of molecules oriented in opposite directions in order to optimize the interaction between the polar groups. In particular, 8CB bilayers are commonly described as *partial*, since the distance d between bilayers is lower than twice the molecular length l (about 1.4 times the length of one molecule for 8CB), differently from smectic types composed by single layers, where d is about as large as l.[51] For a matter of convenience, we refer to molecules forming the sublayers either as *up*(+) or *down*(−) molecules, depending on whether their dipole moment is parallel or antiparallel to the arbitrarily chosen direction of the layer normal. The snapshot in Fig. 9 highlights the interdigitation between *up* and *down* (red and blue) molecules forming the bilayer of the simulated sample. We refer to the positional order parameter of the up or down pair correlation functions $g_{\pm}(z_{12})$ as $\tau_1^{\pm}$. Values of $\tau_1^{\pm}$ calculated by fitting the distribution profiles with Eq. (A13) are reported in Table I. As shown in Fig. 8, both $g_+(z_{12})$ and $g_-(z_{12})$ present the same trend, but they are shifted by a phase factor $q_1\lambda$. Once the values of λ and d have been determined, the bilayer interdigitation ε can be estimated (see the geometric representation of these parameters in Fig. 5).

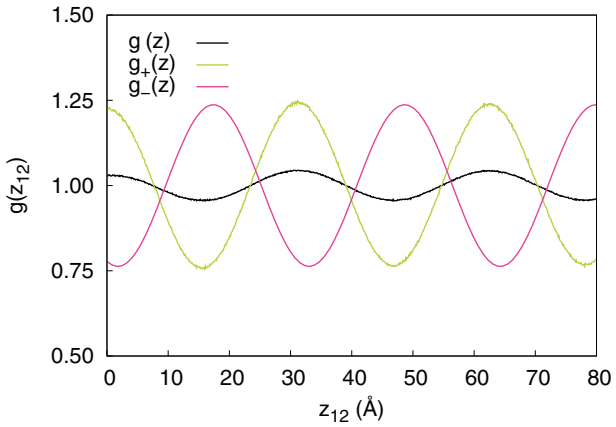

FIG. 8. Comparison of *up* and *down* two particle autocorrelation function $g_{\pm}(z_{12})$ with the one of the whole sample $g(z_{12})$ for system **a**. Here $g_-(z_{12})$ is a best fit function to the actual one which has been shifted of λ so that it yields the total $g(z_{12})$ when combined with $g_+(z_{12})$ (see Eq. (15)).

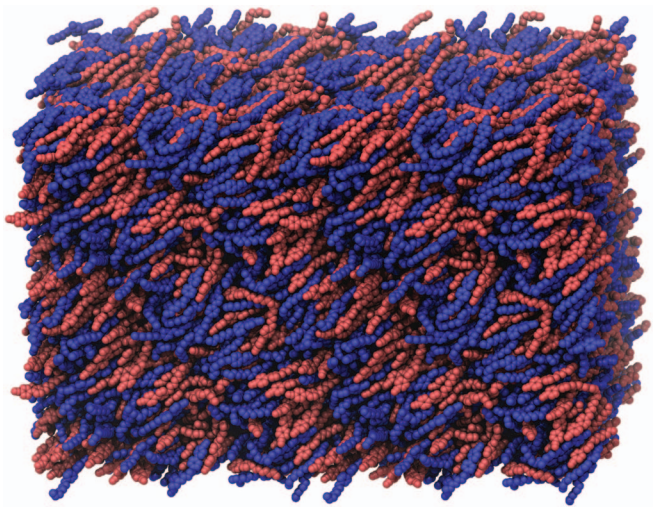

FIG. 9. Layer interdigitation in system **c** (replicated twice along x, y, and z axes). Red and blue colors represent parallel ("up") and antiparallel ("down") molecules.

The total pair correlation function $g(z_{12})$ is then given by the superposition of the *up* and *down* waves, provided they are suitably shifted of $q_1\lambda$:

$$g(z_{12}) = \frac{1}{2}[g_+(z_{12}) + g_-(z_{12}+\lambda)] \approx 1 + (\tau_1^{\pm})^2 \left\{\cos\left[q_1\left(z_{12}-\frac{\lambda}{2}\right)\right] + \cos\left[q_1\left(z_{12}+\frac{\lambda}{2}\right)\right]\right\}. \quad (15)$$

Equation (15) reproduces the pair autocorrelation function of the whole sample (Fig. 8) which possesses a maximum located at $z_{12} = 0$. We then fitted $g_{\pm}(z_{12})$ with Eq. (A13) obtaining the value of $\tau_1^{\pm}$, which was then used as a parameter in Eq. (15) to fit the total pair correlation function,[52] obtaining the values of d, λ and hence the interdigitation ε, reported in Table I. It can be seen that $\tau_1^{\pm}$ is roughly twice τ_1 and that its temperature trend closely follows the one of τ_1. In addition, it must be noted that not only the layer spacing d but also the interdigitation length ε (Fig. 5) is rather constant with the temperature.

G. Mixed order parameters

Although we have discussed orientational and positional orders separately, it is clear that they can, at least in principle, be correlated. Even though various simulations of 8CB have appeared, we are not aware of the mixed orientational positional parameters $p_{L;\,n}$ introduced in Eq. (3), with $L > 0$, $n > 0$ being determined. Here, we wish to provide such an evaluation and use it to test a simple approximation of the mixed parameters as product of the positional and orientational orders.[27]

It is worth recalling that in the first molecular field theory of smectic A liquid crystals proposed by McMillan,[44] which succeeded in qualitatively reproducing the features of smectic A phases, the internal energy of a single molecule was expressed in terms of the orientational and mixed

positional-orientational order parameters and only afterwards, the theory was modified[45] with the introduction of a pure positional order parameter. The averaged internal energy of a single molecule for the coupled model was written by McMillan as

$$U = -u_0(\langle P_2\rangle^2 + \alpha(p_{2;1})^2 + \gamma(\tau_1)^2)/2, \tag{16}$$

where u_0, αu_0, and γu_0 are the strengths of the orientational, mixed, and positional contributions, respectively.

Kventsel *et al.*[27] proposed an alternative simplified theory for smectic A phases, where the mixed order parameter term $p_{2;1}$ was replaced by the product of the positional and orientational order parameters $\langle P_2\rangle\tau_1$.

This decoupled model has the advantage of making the numerical solution of the mean field problem much easier.

Thanks to computer simulations, we can now test if the approximations proposed in the theories were acceptable. In particular, here we can test whether the decoupled model for smectic A phases can describe also the interdigitated smectic A_d phase.

In Table III, we report the values of $p_{L;n} = \langle P_L \cos(q_n z)\rangle$ (see Eq. (3)) (with $n = 1$ and $L = 2, 4$) for the systems with $N = 3000$ and $N = 750$ molecules. It can be seen that for 8CB the orientational and positional orders are actually correlated, with the average of the product $p_{L;n}$ being roughly twice the product of the averages $\langle P_L\rangle\tau_n$. For comparison, we run the same calculation on smectic samples of α-sexithienyl (T6) obtained from a recent work of Pizzirusso *et al.*,[4] revealing that for that system the positional and orientational order parameters are completely decoupled. These results suggest that the approximation of $p_{L;n} = \langle P_L\rangle\tau_n$ which has been used in the Kventsel *et al.* model[27] may not apply to 8CB smectic A_d phase, while it seems to be suitable for simple smectic A phases such as the one of T6. This result points out once again to the important role of simulations, since mixed order parameters are not currently available from experimental measurements.

H. Comparison with experimental positional order

There are very few experimental determinations of positional order, indeed only perhaps a dozen or so, which is surprising considering the hundreds of papers highlighting the interest for smectics. Fortunately 8CB is one of the most studied cases. A first work was that of Leadbetter,[53] which proposed a procedure for obtaining τ_1 from the first reflection peak in a macroscopically unoriented smectic polydomain. More recently, Kapernaum and Giesselmann[48] using X-ray found $\tau_1 = 0.64$–0.74 in the interval T = 309.5–292, while Alexander *et al.*[47] using neutron scattering reported a value of $\tau_1 = 0.46 - 0.57$ in the region T = 293–305. The simulated results for the positional order appear significantly smaller than those obtained from the experimental ones. It is interesting to notice that the positional order obtained from the venerable McMillan theory already mentioned[44] is more similar to the experimental ones than ours, but it is well know that mean field theories overestimate ordering (e.g., even predicting a phase transition in one-dimensional systems, where it does not exist[54]). It is worth examining more in detail some possible sources for the discrepancy with experiment and in particular how the positional order is extracted from scattering measurements.

We start writing the differential elastically scattered cross section per molecule as a sum taken over all the atomic centers and the intensity at scattering vector $\mathbf{q}$ will be proportional to the square of this total wave:

$$I(\mathbf{q}) = \left\langle \left| \sum_{i=1}^{N} \sum_{a\in i} A_{a,i}(\mathbf{q}) \right|^2 \right\rangle \Big/ N \tag{17}$$

$$= k \sum_{i,j=1}^{N} \sum_{\substack{a,b=1 \\ a\in i, b\in j}}^{M} a_{a,i}(q) a^*_{b,j}(q) \langle e^{i[\mathbf{q}\cdot(\mathbf{r}_{a,i} - \mathbf{r}_{b,j})]} \rangle, \tag{18}$$

where k is a proportionality constant and the sum runs on the M atoms a, b belonging to each of the N molecules i and j and positioned at $\mathbf{r}_{a,i}$, $\mathbf{r}_{b,j}$. If we can assume the scattering factors $a_{a,i}(q)$ to be approximately the same for all the relevant

TABLE III. Mixed order parameters $p_{L;n}$ compared to the products of the average order parameters $\langle P_L\rangle\tau_n$. The positional term τ_n and the layer spacing d were computed according to procedure described in Appendix A (method I).

Sample	T (K)	N	$p_{2;1}$	$\langle P_2\rangle\tau_1$	$p_{4;1}$	$\langle P_4\rangle\tau_1$
a	300	750	0.13 ± 0.04	0.08 ± 0.02	0.08 ± 0.03	0.03 ± 0.01
b	300	3000	0.16 ± 0.01	0.09 ± 0.01	0.09 ± 0.01	0.041 ± 0.005
c	300	3000	0.15 ± 0.02	0.09 ± 0.01	0.08 ± 0.01	0.039 ± 0.006
d	310	3000	0.04 ± 0.02	0.017 ± 0.004	0.015 ± 0.008	0.004 ± 0.001
	302	750	0.14 ± 0.03	0.08 ± 0.02	0.08 ± 0.03	0.03 ± 0.01
	304	750	0.13 ± 0.05	0.07 ± 0.02	0.07 ± 0.03	0.03 ± 0.01
	305	750	0.16 ± 0.03	0.09 ± 0.02	0.09 ± 0.02	0.04 ± 0.01
	306	750	0.14 ± 0.03	0.08 ± 0.02	0.08 ± 0.02	0.03 ± 0.01
	307	750	0.13 ± 0.04	0.07 ± 0.02	0.07 ± 0.03	0.03 ± 0.01
	308	750	0.11 ± 0.04	0.06 ± 0.02	0.06 ± 0.04	0.02 ± 0.01
	309	750	0.10 ± 0.03	0.06 ± 0.02	0.05 ± 0.02	0.02 ± 0.01
	310	750	0.08 ± 0.03	0.04 ± 0.02	0.04 ± 0.02	0.012 ± 0.008
	311	750	0.03 ± 0.01	0.006 ± 0.002	0.014 ± 0.008	0.0007 ± 0.0009

atomic centers

$$I(\mathbf{q}) = k|a(\mathbf{q})|^2 S(q), \tag{19}$$

where we have introduced the *structure factor* $S(q)$

$$\begin{aligned} S(q) &= \frac{1}{N}\sum_{i,j=1}^{N}\sum_{\substack{a,b=1\\ a\in i, b\in j}}^{M}\langle e^{i[\mathbf{q}\cdot(\mathbf{R}_{a,i}-\mathbf{R}_{b,j})]}\rangle \\ &= 1 + S_s(q) + S_d(q), \end{aligned} \tag{20}$$

where the second and third terms represent the single molecule ("self") and the pairwise (or "distinct") contributions,

$$S_s(q) = \frac{1}{N}\sum_{i=1}^{N}\sum_{\substack{a,b=1\\ a\neq b\in i}}^{M}\langle e^{i[\mathbf{q}\cdot(\mathbf{R}_{a,i}-\mathbf{R}_{b,i})]}\rangle \tag{21}$$

and

$$S_d(q) = \frac{1}{N}\sum_{\substack{i,j=1\\ i\neq j}}^{N}\sum_{\substack{a,b=1\\ a\in i. b\in j}}^{M}\langle e^{i[\mathbf{q}\cdot(\mathbf{R}_{a,i}-\mathbf{R}_{b,j})]}\rangle. \tag{22}$$

Writing the lab frame position of each atomic center as

$$\mathbf{R}_{a,i} = \mathbf{O}_i + \mathbf{r}_{a,i}, \tag{23}$$

where $\mathbf{O}_i$ is the position of the center of mass of the ith molecule and $\mathbf{r}_{a,i}$ is the position of atom a in the ith molecule fixed frame, we have

$$S_s(q) = \sum_{\substack{a,b=1\\ a\neq b}}^{M}\langle e^{i[\mathbf{q}\cdot(\mathbf{r}_a-\mathbf{r}_b)]}\rangle \tag{24}$$

and

$$S_d(q) = \frac{1}{N}\sum_{\substack{i,j=1\\ i\neq j}}^{N}\sum_{\substack{a,b=1\\ a\in i, b\in j}}^{M}\langle e^{i[\mathbf{q}\cdot(\mathbf{O}_i-\mathbf{O}_j)]}e^{i[\mathbf{q}\cdot(\mathbf{r}_{a,i}-\mathbf{r}_{b,j})]}\rangle. \tag{25}$$

It is clear that the only term containing information relevant for smectic positional order is $S_d(q)$, which depends on molecule-molecule distances. Thus, here we only concentrate on the distinct contribution and in particular, if we now consider the vertical reflections from the smectic planes, $\mathbf{q} = (0, 0, 1)q_n$, $q_n \equiv \frac{2\pi n}{d}$ then

$$S_d(00n) = \frac{1}{N}\sum_{\substack{i,j\\ i\neq j}}^{N}\sum_{\substack{a,b=1\\ a\in i, b\in j}}^{M}\langle e^{iq_n z_{ij}}e^{iq_n[\mathbf{z}\cdot(\mathbf{r}_{a,i}-\mathbf{r}_{b,j})]}\rangle, \tag{26}$$

where $z_{ij} = z_i - z_j$.

Repeated use of the Rayleigh expansion and of the transformation properties of Wigner rotation matrices (see Appendix B) shows that, assuming a uniaxial smectic and effective uniaxial molecular symmetry

$$\begin{aligned} S_d(00n) &= \sum_{L,L'} c_{nLL'}\langle\cos(q_n z_{ij})P_L(\cos\beta_i)P_{L'}(\cos\beta_j)\rangle_{ij} \\ &= c_{n00}\langle\cos(q_n z_{ij})\rangle_{ij} \\ &\quad + 2c_{n02}\langle\cos(q_n z_{ij})P_2(\cos\beta_j)\rangle_{ij} \\ &\quad + c_{n22}\langle\cos(q_m n_{ij})P_2(\cos\beta_i)P_2(\cos\beta_j)\rangle_{ij} + ... \end{aligned} \tag{27}$$

The first term is the only one retained in the classical formulation,[53,55] assuming

$$\langle\cos(q_n z_{ij})\rangle_{ij} = \langle\cos(q_n z_i)\rangle^2. \tag{28}$$

Thus for the first two reflections,

$$S_d(001) \approx c_{100}\tau_1^2, \tag{29}$$

$$S_d(002) \approx c_{200}\tau_2^2, \tag{30}$$

and so on. We see that the root of the difficulty in comparing the simulated data with those obtained from an analysis of scattering data is first in the presence of the scaling factors c_{nJL} and then in the neglect of the mixed positional-orientational terms. Even assuming these to be negligible the determination of the proportionality factor is non-trivial. In a first approach, it was assumed that a calculation could be performed in the limiting case of perfect order.[53] In a more recent method[48] a global fit to different temperatures was performed assuming a Haller type[56] dependence of the smectic order on temperature. In a third case, absolute measurements were performed using small angle neutron scattering.[47] In all these cases, it is clear that a number of assumptions are implied, and that additional terms, such as the mixed order parameters, that we have shown to be non-negligible, should at least in principle have to be considered. Indeed in a recent paper, Gorkunov *et al.*[57] have shown, examining various types of model interaction potentials, that the mixed order parameter may or may not be well approximated as a product of the translational and orientational order parameters and, more importantly, that for some potentials which promote microscale segregation, the mixed order parameter may even be the largest order parameter.

It might thus be that a more refined analysis of X-ray and neutron scattering data might be needed before a comparison between simulated and experimental data that can be considered decisive for the validation of the MD results should be attempted.

I. Translational diffusion

Given the anisotropic nature of the 8CB LC phase, it is of interest to study the dependence of translational diffusion tensor components D_{ii} as a function of the temperature, and hence in each different phase (in particular in the SmA_d one). This can also be of help in order to validate the simulation results through the comparison with experimental data[58] also for the dynamic and not only for the structural aspects.

From simulations, D_{ii} can be calculated from the mean square positional displacements using the classical Einstein

formula

$$D_{ii} = \lim_{t\to\infty} \frac{\langle (R_i(0) - R_i(t))^2 \rangle}{2t}, \tag{31}$$

where R_i is the component of the molecular position vector of each molecule along the axis $i = x, y, z$ of the director frame. In practice, we assume that the asymptotic long time limit and the diffusive regime is reached for values of $t \gtrsim 10$ ns. The parallel and perpendicular diffusion coefficients $D_\parallel$ and $D_\perp$ correspond to D_{zz} and $(D_{xx} + D_{yy})/2$, respectively, while the isotropic diffusion coefficient D_{iso} was calculated as $(D_{xx} + D_{yy} + D_{zz})/3$.

The simulated and experimental isotropic diffusion coefficients follow an Arrhenius temperature dependence:

$$D_{iso} = D_0 e^{-E_a/kT}, \tag{32}$$

where D_0 is the diffusion coefficient for temperature $T \to \infty$ and E_a is the activation energy required for molecules to get over the potential barrier encountered while moving across the sample.

We perform a linear interpolation of the diffusion coefficients reported in Table IV, obtaining a simulated activation energy $E_{a,\,sim} = 34.02$ kJ mol^{-1}, very close to the reported experimental value[58] $E_{a,\,exp} = 34.12$ kJ mol^{-1}, and a $D_{0,\,sim} = 1.97 \times 10^{-4}$ m^2/s against the experimental value we extrapolated from the work of A. Maliniak and co-workers[58] ($D_{0,\,exp} \sim 1.96 \times 10^{-5}$ m^2/s). The D_0 value obtained from UA simulations is thus roughly one order of magnitude higher than the one found experimentally. This is not surprising, as it is well known that for molecules modeled at the united atoms level of detail, the calculated diffusion coefficients are usually higher than experimental values[10,18] as a result of the smoother molecular surface. It is however interesting to see, even if this feature of UA models prevents us from performing a comparison with the absolute values of experimental results, whether we can at least satisfactorily obtain the anisotropy and the temperature dependence of the translational diffusion tensor.

In particular, we tried two scaling procedures that, given a simulated diffusion coefficient, will return a rescaled one directly comparable to experimental values.

(i) The first, very simple, is based on introducing two empirical scaling factors:

$$\alpha = \frac{D_{0,exp}}{D_{0,sim}}, \quad \beta = \frac{E_{a,exp}}{E_{a,sim}}, \tag{33}$$

which in our case correspond to $\alpha = 0.1$ and $\beta = 1.01$, to be employed in the following expression:

$$D_{iso,r} = \alpha e^{(1-\beta)\frac{E_{a,sim}}{kT}} D_{iso,sim}, \tag{34}$$

where $D_{iso,\,r}$ is the simulation-rescaled isotropic diffusion coefficient. We applied Eq. (34) not only to rescale the isotropic diffusion coefficient, but also to the components $D_\parallel$ and $D_\perp$ in the LC phase. It is worth noting that this approach based only on a rescaling of the isotropic diffusion coefficients might fail since, in particular, the Arrhenius equation does not necessarily hold when a liquid crystal phase is present, so that we do not necessarily expect $D_\parallel$ and $D_\perp$ in both nematic and smectic ranges to be represented by the equivalent of Eq. (32). However, as we can see from Fig. 10, in practice the agreement turns out to be quite good.

(ii) The second procedure, that tries to provide a more solid basis for scaling also the diffusion components, is based on the Chu and Moroi (CM) model,[58,59] which allows to compute $D_\parallel$ and $D_\perp$ for nematic phases as a function of the scalar order parameter $\langle P_2 \rangle$, ignored in the previous approach, as follows:

$$D_\parallel = \langle D_{iso} \rangle \left[1 + 2\langle P_2 \rangle \frac{1-\xi}{2\xi + 1} \right] \tag{35}$$

TABLE IV. Simulated values with respect to the temperature of: mass density ρ – nematic order parameter $\langle P_2 \rangle$ – average value of the length to breadth molecular aspect ratio l/w, calculated from the dimensions of the minimal rectangular box containing the molecule rotated in its inertial frame[1] – diffusion coefficients in 10^{-10} m^2/s: isotropic coefficient D_{iso}, rescaled isotropic coefficient $D_{iso,\,r}$, parallel coefficient from rescaled isotropic through CM model $D_{\parallel,\,CM}$, perpendicular coefficient from rescaled isotropic through CM model $D_{\perp,\,CM}$.

T (K)	ρ (g/cm^3)	$\langle P_2 \rangle$	l/w	D_{iso}	$D_\parallel$	$D_\perp$
300	1.000	0.64	3.35	2.6	3.8	1.9
302	0.998	0.62	3.37	2.6	3.9	2.0
304	0.995	0.61	3.36	2.8	4.1	2.1
305	0.993	0.62	3.36	2.8	3.9	2.2
306	0.992	0.59	3.35	3.0	4.4	2.3
307	0.990	0.58	3.34	3.0	4.3	2.3
308	0.988	0.54	3.33	3.3	4.8	2.6
309	0.987	0.56	3.16	3.4	4.9	2.6
310	0.985	0.52	3.32	3.6	5.2	2.8
311	0.982	0.45	3.28	3.8	5.4	3.1
312	0.981	0.43	3.28	4.0	5.5	3.2
313	0.975	0.20	…	4.4	…	…
314	0.973	0.16	…	4.5	…	…
316	0.970	0.14	…	4.8	…	…
320	0.963	0.11	…	5.4	…	…

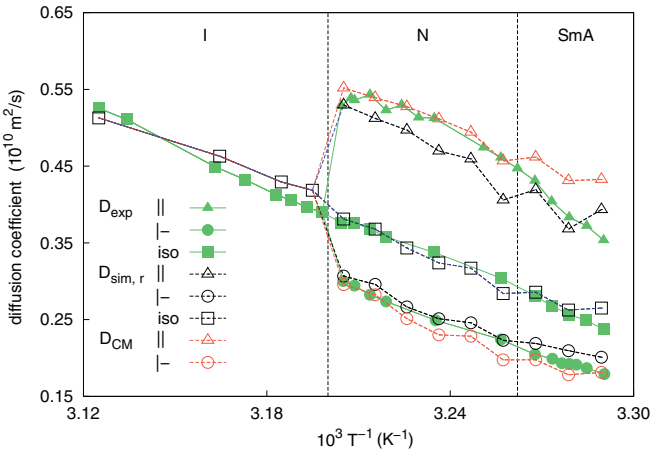

FIG. 10. Arrhenius plot of simulation-rescaled and experimental[58] diffusion coefficients. Green filled symbols represent experimental values, blue empty symbols represent rescaled values from simulations, orange empty symbols represent values calculated with CM model. Dashed lines correspond to experimental transition temperatures.

and

$$D_{\perp} = \langle D_{iso} \rangle \left[1 - \langle P_2 \rangle \frac{1-\xi}{2\xi+1} \right], \tag{36}$$

where $\xi = \pi w/(4l)$ is a geometrical factor for rod-like molecules of length l and section w. Through the CM model, once $D_{iso,\,sim}$, $\langle P_2 \rangle$ and ξ are determined from the simulation at each temperature, we can obtain rescaled parallel and perpendicular diffusion coefficients $D_{\parallel,\,CM}$ and $D_{\perp,\,CM}$ in the nematic phase using Eqs. (34)–(36). It is interesting to see how well the CM model will perform in calculating diffusion coefficients using only orientational order parameter even for samples in the smectic phase, where more complex models taking into account also positional order should in principle be better suited for the task.[60]

In Fig. 10, we report a comparison between the two sets of simulation-rescaled diffusion coefficients and the experimental ones. As shown by the plots, once adequately rescaled, the diffusion coefficients of the simulated samples accurately follow the experimental trend. Moreover, it can be noticed that there is only a slight difference between the values of $D_{\parallel}$ and $D_{\perp}$ calculated from the simple rescaling with Eq. (34) and those predicted by the CM model, the latter method being more effective for $D_{\parallel}$.

Turning now to discussing the mobility results, we see first that, as expected for nematic phases, the diffusion along the director is faster compared to the perpendicular one. This behavior is inherited also in the smectic phase, without showing any evidence of discontinuity in correspondence of the smectic-nematic transition. This trend might seem surprising considering the idealized picture of a smectic phase as a set of stacked two-dimensional fluid layers, as one would expect a lower diffusion along the director and thus across layers, due to the presence of an interlayer potential. On the other hand, it has been reported several times in previous experimental[61–63] and computational[4,15] studies that 8CB exhibits a smectic phase with a nematic-like diffusional behavior and it is comforting to see that this is also reproduced in our work.

IV. CONCLUSIONS

We have investigated the liquid crystalline, nematic and smectic, phases of 4-n-octyl-4′-cyanobiphenyl with atomistic molecular dynamics simulations, by performing a progressive cooling of an isotropic sample. We observed the spontaneous onset of a smectic phase, in a sample composed by 750 molecules with periodic boundary conditions, which we thoroughly investigated and characterized by determining its density, orientational, positional and orientational-positional order parameters. The isotropic-nematic and the nematic-smectic transition temperatures were reproduced in very good agreement with experiment[42] (respectively, within 2 K and 4 K) and a satisfactory agreement with birefringence[37–39] and polarized Raman data[11,40] was also found for the second and fourth rank orientational order parameters $\langle P_2 \rangle$, $\langle P_4 \rangle$.

The determination of the mixed positional-orientational order parameters allowed us to evaluate for the first time the correlation between positions and orientations in smectic phases.

We have also proposed a general protocol for determining the positional order parameter τ_1 for smectic A phases from molecular dynamics simulations and we found that, for both $N = 750$ and various larger, N= 3000 molecules samples with different thermal histories, τ_1 is somewhat lower than the experimental values reported so far from X-ray and neutron scattering measurements.[47,48] We then discussed in detail and obtained, to our knowledge for the first time, some explicit molecular expressions for the quasi-Bragg smectic reflection spots in terms of the order parameters, showing that the expressions typically used in the analysis can be somewhat oversimplified in that they neglect some contributions from mixed positional orientational order parameters. We consider this as a possible source of the apparent imperfect agreement between calculated and experimental τ_1 since on the other hand the layer spacing d exhibited by our samples is in very good agreement with the experimental X-ray values.[21]

As far as dynamics is concerned, we have evaluated the diffusion tensor components for molecular translations inside and across the smectic layers. Although the absolute values of the diffusion coefficients are roughly an order of magnitude larger than experiment, as usually found for united atoms models, we have shown that a simple rescaling can be used to closely reproduce the experimental temperature variation trend[58] of the diffusion tensor components. In particular, we have also observed that the diffusion coefficient across the layers is higher, up to a factor of two, than that for diffusion in the layer, as found experimentally for 8CB.

In summary, we can conclude that the force field developed in Ref. 10 is validated also for reproducing and predicting absolute values of structural data and, up to a scaling factor, translational diffusion for the smectic phase of 8CB. We trust our study will stimulate further investigations of the smectic positional and positional-orientational order parameters, that are key to a full understanding of this important liquid crystal layered phase, but to date much less explored that their orientational counterparts.

ACKNOWLEDGMENTS

We thank G. Tiberio and S. Breuers for some useful discussions, Emilia-Romagna region for a Spinner postgraduate fellowship granted to M.F.P., MIUR PRIN national project "Novel ordered systems for high response molecular devices" for funding this research, and CINECA Supercomputing Center for providing computer time through the ISCRA scheme.

APPENDIX A: CALCULATION OF POSITIONAL ORDER PARAMETERS

In this appendix, we report details of the two procedures we have employed to obtain positional order. To start with, we notice that to correctly determine the positional order of a sample, it is necessary to sample a portion of the system which can faithfully provide the probability distribution of the phase, thus having the same surface area for any value of z,

and possibly containing an integer number of layers. The former condition is satisfied only for a box where the director coincides with one of the Cartesian axis. To overcome this issue, we have replicated the simulation box in order to obtain a quasi-cubical cell. Then we have considered only the molecules enclosed in a cylinder with the long axis parallel to the director contained in the largest sphere inscribed in the replicated cell.

Once selected a meaningful sampling region, we have identified two possible ways to determine the positional order of a smectic sample.

Method I. The instantaneous positional order parameter τ_n (Eq. (12)) can be computed as the sample average,

$$\begin{aligned}\tau_n &= \frac{1}{N}\left|\sum_{j=1}^{N}\exp(iq_nz)\right| \\ &= |\langle\cos(q_nz)\rangle + i\langle\sin(q_nz)\rangle| \\ &= \sqrt{\langle\cos(q_nz)\rangle^2 + \langle\sin(q_nz)\rangle^2}. \end{aligned} \tag{A1}$$

This expression of τ_n takes into account that the density distribution does not necessarily present a maximum at $z = 0$ but, say, at a certain $z = z_0$ unknown to begin with and possibly to change from one instant of time to another. Equation (A1) can be easily proved since

$$\begin{aligned}\langle\cos(q_nz)\rangle &= \int_a^{a+d} P(z+z_0)\cos(q_nz)\,\mathrm{d}z \\ &= \tau_n\cos(q_nz_0), \end{aligned} \tag{A2}$$

$$\begin{aligned}\langle\sin(q_nz)\rangle &= \int_a^{a+d} P(z+z_0)\sin(q_nz)\,\mathrm{d}z \\ &= -\tau_n\sin(q_nz_0), \end{aligned} \tag{A3}$$

for an arbitrary a, suggesting that for each snapshot the instantaneous phase factor can be estimated as

$$q_1z_0 = \frac{1}{n}\mathrm{atan2}\left(\frac{\langle\cos(q_nz)\rangle}{\tau_n}, \frac{\langle\sin(q_nz)\rangle}{\tau_n}\right), \tag{A4}$$

where atan2(y,x) returns the angle between the x-axis and the vector from the origin to (x, y) in the correct quadrant,[64] e.g., for positive arguments atan2(y, x) ≡ atan(y/x).

We can then further average the instantaneous τ_n over the trajectory to obtain the time average value.

While apparently simple, the evaluation of τ_n is not straightforward, since the instantaneous value of the layer spacing d is obviously not known beforehand. To overcome this issue, for each configuration we first evaluate $\langle\cos(2\pi/d')\rangle$ and $\langle\sin(2\pi/d')\rangle$ in terms of an arbitrary tentative layer spacing d', and then scanning d' and using Eq. (A1) we obtain a plot of $\tau_m(d')$. We can then select the value of d' that maximizes $\tau_m(d')$ as the instantaneous layer spacing of the sample (see Fig. 11). In order to justify such procedure, and also to evaluate the presence of errors resulting from the finite size of the sample box, we derive analytical expressions

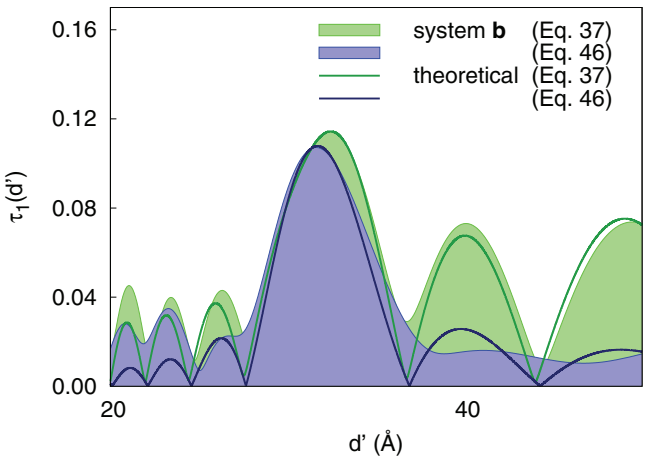

FIG. 11. $\tau_1(d')$ as a function of the trial layer spacing d' for simulated system **b** (color filled regions) and for method I with $\tau_1 = 0.11$, $d = 31.6$ Å, $L = 110$ Å, and $z_0 = 14$ Å, with (blue lines, Eq. (A10)) and without (green lines, Eq. (A1)) removal of the spurious factor.

for $\langle\cos(2m\pi/d')\rangle$ and $\langle\sin(2m\pi/d')\rangle$,

$$\begin{aligned}\left\langle\cos\left(\frac{2m\pi z}{d'}\right)\right\rangle &= \int_a^b\left[\frac{1}{L} + \sum_m\frac{2\tau_n}{L}\cos(q_n(z+z_0))\right] \\ &\quad\times\cos\left(\frac{2\pi mz}{d'}\right)dz \\ &= \frac{1}{q'_mL}\sin(q'_mz)\Big|_a^b \\ &\quad+\sum_{n=1}\frac{\tau_n}{L}\left[\frac{1}{A}\sin(Az+q_nz_0)\right]\Big|_a^b \\ &\quad+\sum_{n=1}\frac{\tau_n}{L}\left[\frac{1}{B}\sin(Bz+q_nz_0)\right]\Big|_a^b, \end{aligned} \tag{A5}$$

$$\begin{aligned}\left\langle\sin\left(\frac{2m\pi z}{d'}\right)\right\rangle &= -\frac{1}{q'_mL}\cos(q'_mz)\Big|_a^b \\ &\quad-\sum_{n=1}\frac{\tau_n}{L}\left[\frac{1}{A}\cos(Az+q_nz_0)\right]\Big|_a^b \\ &\quad+\sum_{n=1}\frac{\tau_n}{L}\left[\frac{1}{B}\cos(Bz+q_nz_0)\right]\Big|_a^b, \end{aligned} \tag{A6}$$

with

$$A = \frac{2\pi(nd'+md)}{dd'}, \quad B = \frac{2\pi(nd'-md)}{dd'}, \tag{A7}$$

where $q'_m = 2\pi m/d'$ and the cell length $L = b - a$, with a and b being the generic cell boundaries.

It can be seen that both $\langle\cos(2m\pi/d')\rangle$ and $\langle\sin(2m\pi/d')\rangle$ are the sum of three terms. The first term arises solely from the finite size of the cell and tends to zero for L tending to infinity. The second term is a function of τ_n but does not show a maximum for integer m and is negligible even at fairly small values of L. The third term is the one responsible for the peaks visible in the plot of $\tau_m(d')$, corresponding to τ_n. This can be

demonstrated by evaluating the limit for $\delta \equiv md' - nd$ tending to zero,

$$\lim_{\delta\to 0}\left\langle \cos\left(\frac{2\pi mz}{d'}\right)\right\rangle = \tau_n \cos(q_n z_0), \tag{A8}$$

$$\lim_{\delta\to 0}\left\langle \sin\left(\frac{2\pi mz}{d'}\right)\right\rangle = -\tau_n \sin(q_n z_0). \tag{A9}$$

This shows that $\tau_m(d')$ has multiple peaks if the phase presents higher order terms of positional order. In particular, $n > m$ and $n < m$ peaks will appear at the left and the right of the one corresponding to the mth order parameter, respectively. In practice, it is convenient to subtract the first term of Eqs. (A5) and (A6) before computing $\tau_n(d')$ since, especially when L is low and not a multiple of d, it can mask the peak corresponding to τ_n. In Fig. 11, the effect of the spurious terms can be observed qualitatively, and it can be seen to affect both the height and the position of the peak.

When computing the positional order parameters from the simulations, it is convenient to consider a virtual cylindrical region going from $-L$ to $+L$. This simplifies the expression for the positional order parameter, that can be calculated as

$$\tau_n(d') = \left\{\left[\left\langle \cos\left(\frac{2n\pi}{d'}\right)\right\rangle - \frac{d'}{2\pi nL}\sin\left(\frac{2\pi nL}{d'}\right)\right]^2 + \left\langle \sin\left(\frac{2n\pi}{d'}\right)\right\rangle^2\right\}^{1/2}. \tag{A10}$$

Additionally, Eqs. (A5) and (A6) suggest that the sharpness of the peaks corresponding to τ_n depends essentially on the length of the sampling region, as L appears in the argument of the cosine and sine functions, increasing the frequency of their oscillations.

It is worth noting that the choice of the computational approach used to obtain the average positional order parameters can influence the estimate of the positional order of a smectic sample. In their works, De Gaetani and Prampolini[17] and Zhang *et al.*[18] determined τ_1 by summing the instantaneous $\tau_1(d')$ plots and taking the maximum value of the resulting averaged plot as τ_1. However, this approach may lead to artificially low values of τ_1. In fact, the instantaneous value of the layer spacing, d', is not constant during the simulation, thus the peaks of $\tau_m(d')$ of different configurations do not superimpose anymore, resulting in lower values of τ_1. To avoid this problem, here we computed τ_1 as the average of the maximum values of the instantaneous $\tau_1(d')$ plot.

This method to evaluate the positional order has the advantage of being computationally inexpensive, since it scales with $O(N)$. Additionally, the evaluation of $\tau(d)$ can be exploited also to compute the average probability density distributions. Since liquid crystal phases are fluid systems and thus the maxima of the density distribution tend to shift during the simulation, we can exploit the phase factor calculated from Eq. (A4) to rephase the instantaneous probability distribution and obtain the average one.

Method II. A second way to estimate the positional order exploits the two particle autocorrelation function $P(z_{12})$, which can be obtained as

$$P(z_{12}) = \int_0^d P(z_1)\cdot P(z_1 - z_{12})\,\mathrm{d}z_1 = \frac{1}{d} + \frac{2}{d}\sum_{n=1}^{\infty}(\tau_n)^2\cos(q_n z_{12}), \tag{A11}$$

with $z_{12} = z_1 - z_2$ being the projection of the intermolecular distance on the layer normal. It is common to express such function as

$$g(z_{12}) = P(z_{12})\,d = \frac{\rho(z_{12})}{\rho_N}. \tag{A12}$$

In the simplest case,[45,65] the normalized autocorrelation function along the layer normal (Fig. 8) described by Eq. (A12) can be truncated to the first term in the Fourier expansion as

$$g(z_{12}) \approx 1 + 2\tau_1^2\cos(q_1 z_{12}). \tag{A13}$$

The values of τ_1 and d can then be extrapolated by least square fitting the $g(z_{12})$ profiles with Eq. (A13).[66]

The correlation function method has three main advantages: (i) it is independent on any phase factor and on the length of the sampling region L, always featuring a maxima at $z_{12} = 0$, (ii) it increases the signal-to-noise ratio, allowing for a more accurate fit, and (iii) it allows to obtain directly both τ_n and the layer spacing d. On the other hand, it scales with $O(N^2)$ and thus is much slower than method I. Hence, its use is recommended only for small samples, where the noise is high and the sampling region is inevitably small.

APPENDIX B: EXPLICIT EXPRESSION FOR SCATTERING COEFFICIENTS IN SMECTIC A

In this appendix, we derive an explicit expression for the distinct molecules contribution to the scattered intensity $S_d(q)$ in the particular case of reflections from the smectic A planes with $\mathbf{q} = (0, 0, 1)q_n$, $q_n \equiv \frac{2\pi n}{d}$, thus assuming that the scattering vector is parallel to the director, $\mathbf{q}||\mathbf{d}$ is (see Eq. (26))

$$S_d(00n) = \frac{1}{N}\sum_{\substack{i,j\\ i\neq j}}^{N}\sum_{a\in i, b\in j}^{M}\langle e^{iq_n z_{ij}} e^{iq_n \mathbf{z}\cdot\mathbf{r}_{a,i}} e^{-iq_n \mathbf{z}\cdot\mathbf{r}_{b,j}}\rangle, \tag{B1}$$

where $z_{ij} = z_i - z_j$.

We use the Rayleigh expansion,

$$e^{i\mathbf{q}\cdot\mathbf{r}_{a,i}} = \sum i^L(2L+1)j_L(qr_{a,i})D^L_{00}(\hat{\mathbf{q}}\cdot\hat{\mathbf{r}}_{a,i}), \tag{B2}$$

with $j_L(qr)$ a spherical Bessel function.[67] Now, applying the closure relation of Wigner rotation matrices we have

$$D^L_{00}(\hat{\mathbf{q}}\cdot\hat{\mathbf{r}}_{ai}) = \sum_m D^L_{0m}(d - r_{ai})D^L_{m0}(q - d) \tag{B3}$$

$$= \sum_m D^{L*}_{m0}(q - d)D^L_{m0}(r_{ai} - d) \tag{B4}$$

$$= \sum_{m,p} D^{L*}_{m0}(q-d)\left\langle D^{L}_{mp}(M_i-d)\right\rangle D^{L}_{p0}(r_{ai}-M_i)$$

$$= \sum_{m,p} \delta_{m0}\left\langle D^{L}_{mp}(M_i-d)\right\rangle D^{L}_{p0}(r_{ai}-M_i)$$

$$= \sum_{p} \left\langle D^{L}_{0p}(M_i-d)\right\rangle D^{L}_{p0}(r_{ai}-M_i). \quad \text{(B5)}$$

where $(M_i - d)$ is the rotation from the lab (director) frame d to the ith molecule frame M_i and $(r_{ai} - M_i)$ the rotation from the molecular frame to scattering center a. In particular, for our geometry we have used $D^{L*}_{m0}(0) = \delta(m0)$,

$$\langle e^{iq_n z_{ij}} e^{i\mathbf{q_n}\cdot\mathbf{r}_{a,i}} e^{i\mathbf{q_n}\cdot\mathbf{r}_{b,j}}\rangle = \sum i^{L+L'}(2L+1)(2L'+1)$$
$$j_L(q_n r_{a,i}) j'_L(q_n r_{b,j})$$
$$\sum_{p,p'} D^{L}_{p0}(r_{ai}-M_i) D^{L'}_{p'0}(r_{bj}-M_j)$$
$$\langle \cos(q_n z_{ij}) D^{L}_{0p}(M_i - d) D^{L}_{0p'}(M_j - d)\rangle. \quad \text{(B6)}$$

If the molecules are all identical, the position and orientations of the center depend on internal geometry and we can just write $r_{a,i} = r_a$, $D^{L}_{p0}(r_{ai} - M_i) = D^{L}_{p0}(r_a - M)$, etc. Introducing a molecular scattering tensor of rank L:

$$A^{L,p}(q) = \sum_{a=1}^{M} i^L (2L+1) j_L(q r_a) D^{L}_{p0}(r_a - M), \quad \text{(B7)}$$

we can write

$$S_d(00n) = \sum_{L,L'} \sum_{p,p'} A^{L,p}(q_n) A^{L',p'}(q_n)$$
$$\langle \cos(q_n z_{ij}) D^{L}_{0p}(M_i - d) D^{L'}_{0p'}(M_j - d)\rangle_{ij}, \quad \text{(B8)}$$

where we have indicated the average over all particle pairs as $\langle[\ldots]\rangle_{ij}$. Assuming an effective uniaxial molecular symmetry, invariance about a rotation around the molecular axis gives $\delta_{p0}\delta_{p'0}$. Thus

$$S_d(00n) = \sum_{L,L'} A^{L,0}(q_n) A^{L',0}(q_n)$$
$$\langle \cos(q_n z_{ij}) P_L(\cos\beta_i) P_{L'}(\cos\beta_j)\rangle_{ij}, \quad \text{(B9)}$$

where we have used the familiar notation $P_L(\cos\beta_i) \equiv D^{L}_{00}(M_i - d)$. We can thus write explicitly the coefficients in Eq. (28) as

$$c_{nLL'} = A^{L}(q_n) A^{L'}(q_n). \quad \text{(B10)}$$

[1] R. Berardi, L. Muccioli, and C. Zannoni, ChemPhysChem **5**, 104 (2004).
[2] Y. Olivier, L. Muccioli, V. Lemaur, Y. H. Geerts, C. Zannoni, and J. Cornil, J. Phys. Chem. B **113**, 14102 (2009).
[3] T. A. Papadopoulos, L. Muccioli, S. Athanasopoulos, A. B. Walker, C. Zannoni, and D. Beljonne, Chem. Sci. **2**, 1025 (2011).
[4] A. Pizzirusso, M. Savini, L. Muccioli, and C. Zannoni, J. Mater. Chem. **21**, 125 (2011).
[5] I. Cacelli, C. F. Lami, and G. Prampolini, J. Comput. Chem. **30**, 366 (2009).
[6] J. Peláez and M. R. Wilson, Phys. Rev. Lett. **97**, 267801 (2006).
[7] C. Zannoni, J. Mater. Chem. **11**, 2637 (2001).
[8] M. R. Wilson, Chem. Soc. Rev. **36**, 1881 (2007).
[9] I. Cacelli, L. De Gaetani, G. Prampolini, and A. Tani, J. Phys. Chem. B **111**, 2130 (2007).
[10] G. Tiberio, L. Muccioli, R. Berardi, and C. Zannoni, ChemPhysChem **10**, 125 (2009).
[11] S. J. Picken, "Measurements and values for selected order parameters," in *Physical Properties of Liquid Crystals, Vol. 1: Nematics*, edited by D. A. Dunmur, A. Fukuda, and G. R. Luckhurst (IEE, London, 2001), Chap. 2.2, p. 89.
[12] A. Sanchez-Castillo, M. A. Osipov, and F. Giesselmann, Phys. Rev. E **81**, 021707 (2010).
[13] A. Pizzirusso, M. B. Di Cicco, G. Tiberio, L. Muccioli, R. Berardi, and C. Zannoni, J. Phys. Chem. B **116**, 3760 (2012).
[14] A. C. J. Weber, A. Pizzirusso, L. Muccioli, C. Zannoni, W. L. Meerts, C. A. de Lange, and E. E. Burnell, J. Chem. Phys. **136**, 174506 (2012).
[15] Y. Lansac, M. A. Glaser, and N. A. Clark, Phys. Rev. E **64**, 051703 (2001).
[16] A. J. McDonald and S. Hanna, J. Chem. Phys. **124**, 164906 (2006).
[17] L. De Gaetani and G. Prampolini, Soft Matter **5**, 3517 (2009).
[18] J. Zhang, J. Su, and H. Guo, J. Phys. Chem. B **115**, 2214 (2011).
[19] D. Frenkel and B. Smit, *Understanding Molecular Simulations: From Algorithms to Applications* (Academic Press, San Diego, 1996).
[20] A. J. Leadbetter, J. C. Frost, J. P. Gaughan, G. W. Gray, and A. Mosley, J. Phys. **40**, 375 (1979).
[21] S. Urban, J. Przedmojski, and J. Czub, Liq. Cryst. **32**, 619 (2005).
[22] T. A. Krentsel Lobko, O. D. Lavrentovich, and S. Kumar, Mol. Cryst. Liq. Cryst. **304**, 463 (1997).
[23] M. G. Martin and J. I. Siepmann, J. Phys. Chem. B **102**, 2569 (1998).
[24] F. Chami, M. R. Wilson, and V. S. Oganesyan, Soft Matter **8**, 6823 (2012).
[25] M. Hird, "Relationship between molecular structure and transition temperatures for calamitic structures in nematics," in *Physical Properties of Liquid Crystals: Nematics*, edited by D. A. Dunmur, A. Fukuda, and G. R. Luckhurst (INSPEC/IEE, 2001), Vol. 25, p. 3.
[26] M. J. Cook and M. R. Wilson, Liq. Cryst. **27**, 1573 (2000).
[27] G. F. Kventsel, G. R. Luckhurst, and H. B. Zewdie, Mol. Phys. **56**, 589 (1985).
[28] W. D. Cornell, P. Cieplak, C. I. Bayly, I. R. Gould, K. M. Merz, D. M. Ferguson, D. C. Spellmeyer, T. Fox, J. W. Caldwell, and P. A. Kollman, J. Am. Chem. Soc. **117**, 5179 (1995).
[29] J. Wang, P. Cieplak, and P. A. Kollman, J. Comput. Chem. **21**, 1049 (2000).
[30] J. Peláez and M. R. Wilson, Phys. Chem. Chem. Phys. **9**, 2968 (2007).
[31] J. C. Phillips, R. Braun, W. Wang, J. Gumbart, E. Tajkhorshid, E. Villa, C. Chipot, R. D. Skeel, L. Kale, and K. Schulten, J. Comput. Chem. **26**, 1781 (2005).
[32] H. J. C. Berendsen, J. P. M. Postma, W. F. van Gunsteren, A. Di Nola, and J. R. Haak, J. Chem. Phys. **81**, 3684 (1984).
[33] U. Essmann, L. Perera, M. L. Berkowitz, T. A. Darden, H. Lee, and L. G. Pedersen, J. Chem. Phys. **103**, 8577 (1995).
[34] A. Wuerflinger and M. Sandmann, "Equations of state for nematics," in *Physical Properties of Liquid Crystals, Vol. 1: Nematics*, edited by D. A. Dunmur, A. Fukuda, and G. R. Luckhurst (IEE, London, 2001), Chap. 3.3, p. 151.
[35] C. Zannoni, "Distribution function and order parameters," in *The Molecular Physics of Liquid Crystals*, editey by G. R. Luckhurst and G. W. Gray (Academic Press, London, 1979), p. 51.
[36] P. J. Wojtowicz, "Introduction to the molecular theory of smectic-A liquid crystals," in *Introduction to Liquid Crystals* edited by E. B. Priestley, P. J. Wojtowicz, and P. Sheng (Plenum Press, 1975), p. 83.
[37] *Physical Properties of Liquid Crystals, Vol. 1: Nematics*, EMIS Datareview Series Vol. 25, edited by D. A. Dunmur, A. Fukuda, and G. R. Luckhurst (IEE, London, 2001).
[38] R. G. Horn, J. Phys. **39**, 105 (1978).
[39] I. Chirtoc, M. Chirtoc, C. Glorieux, and J. Thoen, Liq. Cryst. **31**, 229 (2004).
[40] H. F. Gleeson, C. D. Southern, P. D. Brimicombe, J. W. Goodby, and V. Görtz, Liq. Cryst. **37**, 949 (2010).
[41] U. Fabbri and C. Zannoni, Mol. Phys. **58**, 763 (1986).
[42] *The Molecular Physics of Liquid Crystals*, edited by G. R. Luckhurst and G. W. Gray (Academic Press, London, 1979).
[43] F. Gillot, F. O. Morin, H. F. Arata, R. Guegan, H. Tanaka, and H. Fujita, Lab on a Chip **7**, 1600 (2007).
[44] W. L. McMillan, Phys. Rev. A **4**, 1238 (1971).
[45] W. L. McMillan, Phys. Rev. A **6**, 936 (1972).

[46]M. Fukuto, O. Gang, K. J. Alvine, B. M. Ocko, and P. S. Pershan, Phys. Rev. E **77**, 031607 (2008).
[47]G. G. Alexander, S. M. King, R. M. Richardson, and H. Zimmermann, Liq. Cryst. **37**, 961 (2010).
[48]N. Kapernaum and F. Giesselmann, Phys. Rev. E **78**, 062701 (2008).
[49]C. Zhang, M. Gao, N. Diorio, W. Weissflog, U. Baumeister, S. Sprunt, J. T. Gleeson, and A. Jakli, Phys. Rev. Lett. **109**, 107802 (2012).
[50]Y. G. J. Lau, R. M. Richardson, and R. Cubitt, J. Chem. Phys. **124**, 234910 (2006).
[51]P. Pasini and C. Zannoni, *Advances in the Computer Simulations of Liquid Crystals* (Kluwer Academic Publishers, 1998), p. 296.
[52]An estimate of τ_1 can be obtained directly from $\tau_1^{\pm}$, knowing λ and d, by combining Eqs. (15) and (A13): $\tau_1 = \tau_1^{\pm}\sqrt{\cos(\frac{\pi\lambda}{d})}$.
[53]A. J. Leadbetter, "Structural studies of nematic, smectic A and smectic C phases," in *The Molecular Physics of Liquid Crystals*, edited by G. R. Luckhurst and G. Gray (Academic Press, London, 1979), p. 285.
[54]L. P. Kadanoff, J. Stat. Phys. **137**, 777–797 (2009).
[55]J. M. Seddon, "Structural studies of liquid crystals by X-ray diffraction," in *Handbook of Liquid Crystals*. *Low Molecular Weight Liquid Crystals II*, edited by D. Demus, J. Goodby, G. W. Gray, H.-W. Spiess, and V. Vill (Wiley-VCH, 1998), Vol. 2B, p. 635.
[56]I. Haller, Prog. Solid State Chem. **10**, 103 (1975).
[57]M. V. Gorkunov and M. A. Osipov, Phys. Rev. E **84**, 051704 (2011).
[58]S. V. Dvinskikh, I. Furó, H. Zimmermann, and A. Maliniak, Phys. Rev. E **65**, 061701 (2002).
[59]K. S. Chu and D. S. Moroi, J. Phys. Colloq. **36**, C1-99 (1975).
[60]F. Volino and A. J. Dianoux, Mol. Phys. **36**, 389 (1978).
[61]S. Miyajima, A. F. McDowell, and R. M. Cotts, Chem. Phys. Lett. **212**, 277 (1993).
[62]G. J. Krüger, H. Spiesecke, and R. V. Steenwinkel, J. Phys. Colloq. **37**, C3-123 (1976).
[63]M. P. Lettinga and E. Grelet, Phys. Rev. Lett. **99**, 197802 (2007).
[64]Further details on the two-argument arctangent function atan2 available at http://en.wikipedia.org/wiki/Atan2.
[65]R. G. Marguta, E. Martín del Río, and E. de Miguel, J. Phys.: Condens. Matter **18**, 10335 (2006).
[66]The values reported as τ_1 in Refs. 3 and 4 correspond to the present $2(\tau_1)^2$.
[67]M. Abramowitz and I. A. Stegun, *Handbook of Mathematical Functions* (Dover, New York, 1965).